Hindawi
Journal of Control Science and Engineering
Volume 2021, Article ID 2744193, 12 pages
https://doi.org/10.1155/2021/2744193

Research Article

Fault Frequency Identification of Rolling Bearing Using Reinforced Ensemble Local Mean Decomposition

Bo Qin,[1,2] Quanyi Luo,[1] Juanjuan Zhang,[3] Zixian Li,[1,4] and Yan Qin[5]

[1]*School of Mechanical Engineering, Inner Mongolia University of Science and Technology, Baotou, China*
[2]*Mining Research Institute, Inner Mongolia University of Science and Technology, Baotou, China*
[3]*Baotou Vocational and Technical College, Baotou, China*
[4]*State Key Laboratory of Mechanical Transmissions, Chongqing University, Chongqing, China*
[5]*School of Electrical and Electronic Engineering, Nanyang Technological University, Singapore*

Correspondence should be addressed to Yan Qin; yan.qin@ntu.edu.sg

Received 30 July 2021; Revised 29 October 2021; Accepted 25 November 2021; Published 29 December 2021

Academic Editor: Manuel Pineda-Sanchez

The vibration signal of rolling bearing exhibits the characteristics of energy attenuation and complex time-varying modulation caused by the transmission with multiple interfaces and complex paths. In view of this, strong ambient noise easily masks faulty signs of rolling bearings, resulting in inaccurate identification or even totally missing the real fault frequencies. To overcome this problem, we propose a reinforced ensemble local mean decomposition method to capture and screen the essential faulty frequencies of rolling bearing, further boosting fault diagnosis accuracy. Firstly, the vibration signal is decomposed into a series of preliminary features through ensemble local mean decomposition, and then the frequency components above the average level are energy-enhanced. In this way, principal frequency components related to rolling bearing failure can be identified with the fast spectral kurtosis algorithm. Finally, the efficacy of the proposed approach is verified through both a benchmark case and a practical platform. The results show that the selected fault characteristic components are accurate, and the identification and diagnosis of rolling bearing status are improved. Especially for the signals with strong noise, the proposed method still could accurately diagnose fault frequency.

1. Introduction

With the merits of low skin friction drag, high rotation speed, and standardized size, rolling bearings, referred to as ball bearings, have been extensively deployed in mechanical transmission systems [1], including but not limited to high-speed trains, vehicles, and wind turbines. Usually, the rolling bearings are used in harsh conditions, such as frequent turn on and off, time-varying load, and so on. Consequently, coupled with multiple negative factors, these complex working conditions make the cages, inner raceways, and outer rollers of rolling bearings prone to fall into failure. Periodic damages caused by the contact force between parts of a rolling bearing lead to the evolution of failures, leading to fatigue damage of the entire transmission system, causing substantial economic losses and even significant safety accidents. According to AlShalalfeh and Shalalfeh [2], 30% of rotating machinery failures could be attributed to rolling bearing failures. Therefore, it becomes an urgent demand for a timely and accurate health evaluation method for rolling bearing, providing safe and efficient operation of the concerned transmission system.

In practice, vibration test analysis has been widely used in identifying the possible faulty type of rolling bearings [3–5]. To determine the location and degree of rolling bearing failure, it extracts fault frequency from the abundant state information in the measured vibration signal. However, vibration signals of rolling bearings measured on industrial sites show energy attenuation and complex time-varying modulation characteristics after being transmitted through multiple interfaces and complex paths. As a result, the essential components of early failures are often

submerged in strong background noise. When the signal-to-noise ratio (SNR) is low, the accuracy of subsequent fault diagnosis is often unsatisfactory. The key to improving its fault diagnosis accuracy is how to accurately extract and locate the components containing sensitive fault characteristic frequencies from the rolling bearing vibration signal.

At the early stage, the empirical mode decomposition (EMD) method proposed by Huang et al. [6] has been widely adopted for frequency decomposition. EMD decomposed the original signal into a limited number of components ranging from high frequency to low frequency. However, the performance of EMD may be discounted due to mode mixing and the end-point effect [7]. To solve the problems of modal mixing and end-point effect of EMD, Jonathan [8] proposed a local mean decomposition (LMD) method, which adaptively converted a nonstationary signal with time-varying frequencies into the sum of a finite number of instantaneous frequency product functions (PFs). Each PF component is the product of an envelope signal and a frequency modulation (FM) signal. Also, the envelope represents the instantaneous amplitude of the PF component, and the FM signal is the instantaneous frequency of the PF component. As extreme points and uneven distributions exist, LMD may lead to discontinuity of the signal, which may lead to the same PF component decomposed from LMD containing both high and low frequencies. As a result, LMD cannot thoroughly solve the modal mixing problem. Recently, the ensemble local mean decomposition (ELMD) algorithm-based fault diagnosis methods [9–12] are increasingly popular and have become the mainstream for vibration signal decomposition. Specifically, the measured vibration signal will be decomposed into a finite series of components with specific frequency and amplitude. These components have complete time-frequency distributions and contribute to the further development of fault diagnosis models. Adding white noise to the original signal increases the continuity of LMD, and the essence of ELMD is to utilize the statistical characteristics of Gaussian white noise in both time space and frequency space. Since the white noise added at each time is random, the PF components obtained by ELMD will be averaged to derive the final decomposition results. Although ELMD could provide feature decomposition of the vibration signal, the decomposed components that are responsible for the real fault of rolling bearings have not been clearly revealed. If insensitive components related to failure have been directly adopted, they will deteriorate the fault diagnosis model. Especially, rolling bearings are used in variable working conditions, in which the speed and torque of the rolling bearing always vary frequently. Consequently, the vibration signal has the characteristics of time-varying and complex frequency and amplitude. This dramatically increases the complexity in decomposing faulty frequency from the concerned signal. It is necessary to filter out unimportant features and retain crucial components regarding early faults from the components obtained from ELMD. To alleviate this problem, some works [13, 14] relied on human experience to select corresponding components decomposed by ELMD, which may be inaccurate. Alternatively, Wang et al. [15] selected PF components presenting fault features with the fast peak diagram. Zhang and Zhou [16] combined the kurtosis and energy information to construct the fault feature. He and Zhou [17] adopted the Kullback–Leibler divergence-based adaptive method to select the proper PF components. Wang et al. [18] applied singular value decomposition to determine the sensitive PF components. Although the methods mentioned above contribute to selecting valuable components, the influence of ambient noise has not yet been considered. Consequently, it is difficult to identify all crucial components containing faulty frequencies accurately.

To solve the challenges mentioned above, this paper proposes a reinforced ELMD method to accurately determine the crucial components. First, we decompose the vibration signal through ELMD to obtain a series of components corresponding to different frequencies. Further, to distinguish the unimportant components from important ones, a two-step screening strategy is proposed. The first step augments the energy of components above the average, highlighting the specific frequency components. In the second step, the fast spectral kurtosis diagram algorithm is adopted to calculate the center frequency and bandwidth corresponding to the maximum kurtosis, serving as a metric to filter out components irrelevant to the fault signal. Based on this, this method is capable of not only identifying components containing faulty frequencies but also enhancing their power. The main contributions of the article have been summarized as follows:

(1) We have augmented the energy of decomposed components corresponding to specific frequency components.

(2) We have adopted the fast spectral kurtosis diagram to calculate the center frequency and bandwidth corresponding to the maximum kurtosis.

(3) We have verified the efficacy of the proposed method through extensive experiments, including both numerical and experimental cases.

The rest of this article is structured as follows. In Section 2, the detailed process of the reinforced ELMD approach is illustrated. Section 3 verifies the efficacy of the proposed method through a benchmark case and a practical experiment system. Finally, Section 4 draws the conclusion.

2. Methodology

Although ELMD could effectively alleviate the problem of modal mixing compared with LMD during the vibration signal decomposition, it cannot clearly explain the correlations between obtained PF components and fault features. As a result, partial PF components are noncrucial and may lead to performance degradation if they are directly applied without further filtering. The energy of corresponding faulty components may be weak compared to the strong ambient noise in the early failure of the rolling bearing. That is, it is challenging to select the fault frequency of the vibration signal accurately. To solve this difficulty, we propose an enhancement strategy to find the crucial and sensitive faulty components. The specifics of the algorithm are sketched in

Figure 1, which mainly includes three parts. The first part is the initial feature decomposition using ELMD. Next, the extracted PF components are further enhanced with a novel mechanism. To select the proper PF components after enhancement, a comparison between center frequency bands calculated with FSK and the frequency of each PF component is conducted in the third part. More details of the proposed method will be specified in the following sections.

2.1. Initial Feature Decomposition Using ELMD. For a given collection of vibration signal $X(t)$, a finite number of instantaneous frequencies could be decomposed by the LMD algorithm, as shown in equation (1). Each PF component is obtained by the product of an envelope signal $a_n(t)$ and a pure frequency modulation signal $s_n(t)$. Then, the complete time-frequency distribution of $X(t)$ can be obtained by summing the above-decomposed components as follows:

$$\begin{aligned} X(t) &= \sum_{n=1}^{N} a_n(t)s_n(t) + u(t), \\ &= \sum_{n=1}^{N} P_n(t) + u(t) \quad (n \in [1, N]), \end{aligned} \tag{1}$$

where P_n is the n^{th} PF component obtained after LMD and $u(t)$ is the residue.

To alleviate the problem of modal mixing in LMD mentioned above, Gaussian white noise $e_i(t)$ will be added in equation (1) to improve the generation ability, which is the basic idea of ELMD. As shown in Figure 2, the detailed process of the feature decomposition of the rolling bearing vibration signal $X(t)$ based on ELMD is summarized below.

Step 1: assuming that the signal $X(t)$ is repeated M times with different randomly sampled Gaussian white noise $e_m(t)$, the mixture signal is presented as follows:

$$X_m(t) = X(t) + e_m(t) \quad (m \in [1, M]), \tag{2}$$

where $X_m(t)$ is the m^{th} mixed signal and $X(t)$ has the same meaning as that given in equation (1).

Step 2: perform ELMD on the mixed signal $X_m(t)$ and obtain N PF components and the residual $u_m(t)$:

$$X_m(t) = P_{1,m}(t) + P_{2,m}(t) + \cdots + P_{N,m}(t) + u_m(t), \tag{3}$$

where $P_{n,m}$ is the n^{th} PF component in the m^{th} decomposition after adding white noise to $X_m(t)$.

Step 3: average the same batch of PF components obtained under different noise backgrounds, as shown in the red dashed box in Figure 2. The final n^{th} component $P_n(t)$ is calculated as the mean value of all components across M times:

$$\begin{aligned} \mathbf{P}_n(t) &= \frac{1}{M}\left[\mathbf{P}_{n,1}(t) + \mathbf{P}_{n,2}(t) + \cdots + \mathbf{P}_{n,M}(t)\right], \\ &= \frac{1}{M}\sum_{m=1}^{M} \mathbf{P}_{n,m}(t). \end{aligned} \tag{4}$$

2.2. Enhancement of the Initial Components. Generally, the mean value of the vibration signal reflects the average level of the corresponding energy. Many unexpected factors, including surface waviness, surface roughness, raceway misalignment, etc., will cause periodic changes of the contact force between parts of rolling bearing [19–21]. The periodic changes will lead to periodic shocks and make the instantaneous amplitude of the vibration signal significantly higher than its average. Taking advantage of these characteristics, an enhancement strategy is proposed here to reinforce the influential components of the vibration signal. The energy of the corresponding component is enlarged by squaring the weak impact component above the average of the vibration signal under strong background noise transmitted through multiple interfaces. The specific calculation procedure is shown below:

$$\widetilde{x}_{i,n} = \frac{\left(nx_{i,n} - \sum x_{i,n}\right)^2}{n\sum|x_i|} \quad (i \in [1, I], n \in [1, N]), \tag{5}$$

where $x_{i,n}$ is the value of the sample with the i^{th} point in the n^{th} feature, I is the number of sampling points in $X(t)$, and $\widetilde{x}_{i,n}$ is the value after feature enhancement.

Taking a period of sinusoidal vibration signal as shown in Figure 3 as an example, it is employed to illustrate the basic idea of feature enhancement. In Figure 3, the blue dotted curve represents the original signal, and the red dotted curve stands for the enhanced signal. Using equation (5) to square the samples above the mean in the original signal to enlarge the energy, we enhance the originally weak fault features. For instance, the value of peak changes from x_i to $\widetilde{x}_i$ after enhancement, making the screening of components more precise.

2.3. Selection of Crucial Components Using FSK. Although kurtosis information is insensitive to the varying load, working speed, size, etc., it is susceptible to shock signals. Out of this consideration, the kurtosis index is suitable for detecting shock faults, widely observed in early rolling bearing faults. For the fault-free situation of a rolling bearing, the amplitude distribution of the vibration signal is close to the normal distribution, and the value of the kurtosis index is chosen as 3. With the varying working conditions and the increases of service time, the distribution of the vibration signal deviates from normal distribution once it steps into failure. Correspondingly, the normal curve is skewed or scattered, and the kurtosis value increases accordingly. The larger the value of the kurtosis, the more serious the failure of the bearing from its normal state. Antoni and Randall [22] proposed the FSK method by dividing the original signal frequency band hierarchically and estimating the kurtosis value of each frequency band. Through iteratively updating, frequency bands with large kurtosis and crucial components will be located. The specific calculation is shown below:

$$K(f) = \frac{\left\langle \left| c_k^i(t) \right|^4 \right\rangle}{\left\langle \left| c_k^i(t) \right|^2 \right\rangle^2} - 2 \quad \left(i \in \left[0, 2^k - 1\right]\right), \tag{6}$$

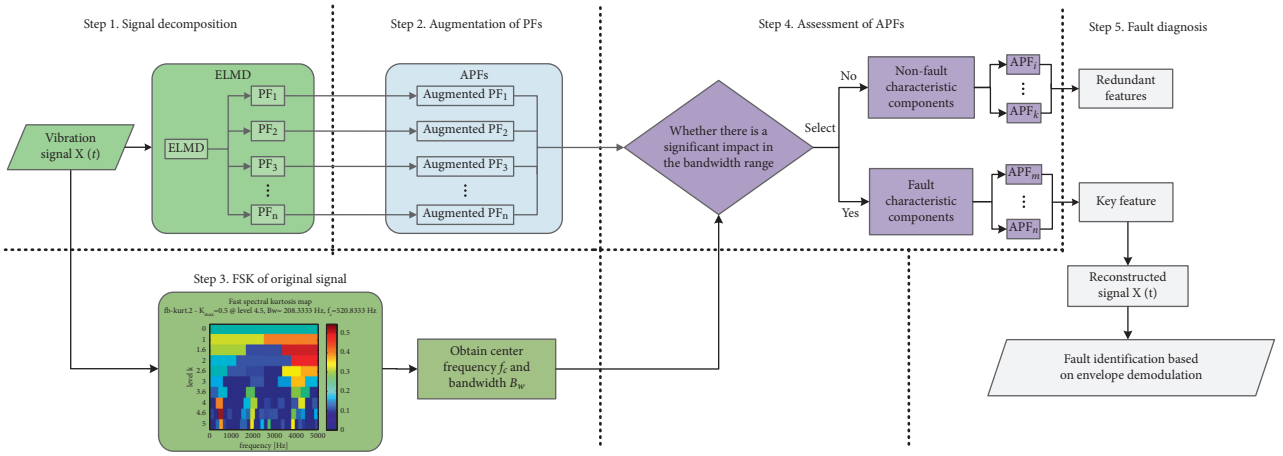

FIGURE 1: The architecture and flowchart of the proposed method.

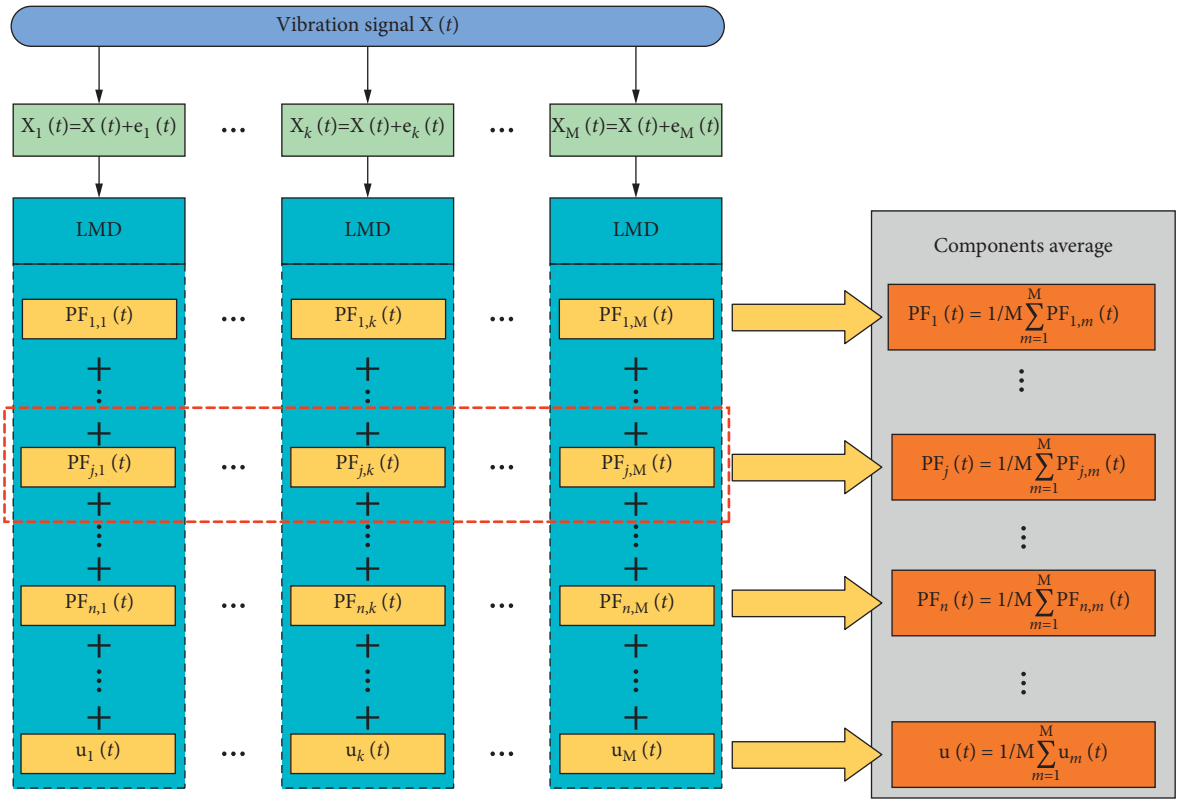

FIGURE 2: The main steps of decomposing enhanced PF components with the proposed approach.

where $K(f)$ calculates the kurtosis value of a specific frequency f, $c_k^i(t)$ is the output of the i^{th} filter of the k^{th} layer, $\langle\cdot\rangle$ denotes modulus value, and $|\cdot|$ stands for expectation.

To improve the screening efficiency of the frequency components of the faulty rolling bearing, FSK is utilized to divide the frequency band of the vibration signal with the enhanced RPF components. The kurtosis value of the vibration signal frequency band is used to characterize the impact degree. Consequently, sensitive impact components of the vibration signal are quickly and effectively screened out. The specific steps are summarized below:

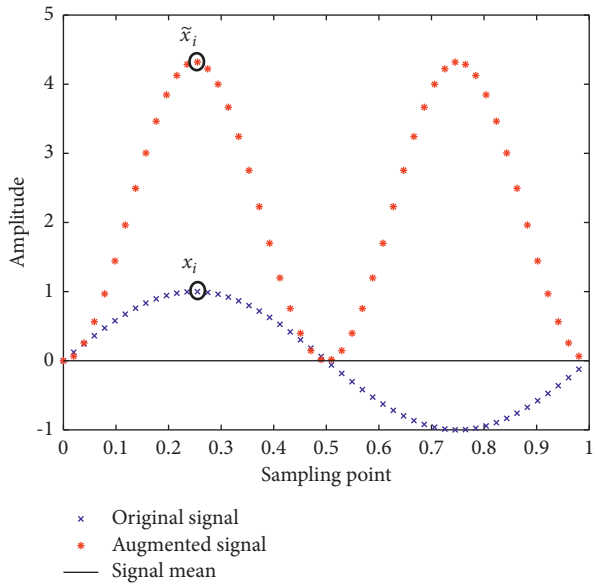

Figure 3: Flow diagram of the proposed fault diagnosis methodology.

Step 1: calculation of FSK values of the original signal.

Performing FSK on $X(t)$, the frequency range of the fault is obtained according to the calculated center frequency f_c and bandwidth B_w.

Step 2: assessment of RPFs.

With the frequency band calculated in the last step, judge whether there are important components by analyzing the spectrum of RPFs. The RPF with concentrated energy is defined as a sensitive fault component.

3. Results and Discussion

This section verifies the efficacy of the proposed method through two cases. The first one is a benchmark provided by the Case Western Reserve University (CWRU) [23–25]. The second one is a self-built test platform to measure the vibration signal of the rolling bearing. The detailed information about data processing, testing result, and conclusion will be carefully illustrated in the following sections.

3.1. Benchmark Case from Case Western Reserve University. Rolling bearing data from CWRU are open-access and freely available. The experimental data are measured from a deep groove ball bearing with the type JEM SKF 6205-2RS. The detailed information about the ball bearing is listed in Table 1. To simulate the real fault, a damage point with a diameter of 0.36 mm is manufactured by the electric discharging machining technique into the inner ring of the bearing ball. Besides, the motor speed is set to be r = 1730 r/minute, and the sampling frequency is 12000 Hz.

A total of 4096 sampling points of the ball bearing were collected to test the performance of the proposed method. Figure 4 shows the time-domain waveform of the measured signal for intuitive understanding. According to the

Table 1: Specifications of JEM SKF 6205-2RS deep groove ball bearing with inner ring fault.

Parameter name and symbol	Value	Unit
Bearing inner diameter	25.00	mm
Bearing outer diameter	52.00	mm
Number of rolling elements (E)	9.00	1
Rolling element diameter (d)	7.90	mm
Pitch circle diameter (D)	39.00	mm
Contact angle (α)	0.00	degree

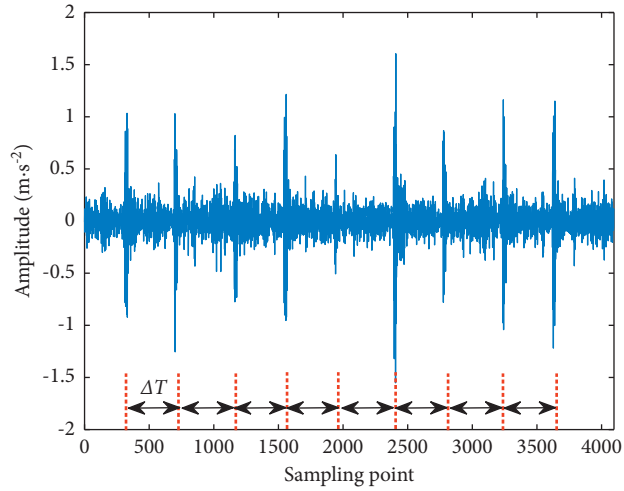

Figure 4: The time-domain trend of the employed data collected from SKF 6205-2RS deep groove ball bearing with inner ring fault.

processing procedure given in Sections 2.1 and 2.2, crucial components of the faults are determined as follows:

(1) Perform ELMD on the time-domain signal collected from SKF 6205-2RS deep groove ball bearing and obtain six PF components.

(2) Calculate the frequency spectrum of each PF component, as shown in Figure 5.

(3) Enhance all the six PF components according to equation (5) and obtain the frequency spectrum of the enhanced RPF components, as shown in Figure 6.

(4) Perform FSK on a time-domain signal with inner ring fault, as shown in Figure 7.

As shown in Figure 7, it is observed that the center frequency f_c and the frequency band B_w corresponding to the maximum kurtosis $K_{\max}$ (13.30) are 800.00 Hz and 106.67 Hz, respectively. Correspondingly, the frequency band range is [693.33 Hz, 906.67 Hz] marked in the black dashed box as shown in Figure 7. By comparing the RPF components in Figure 6, three components RPF_1, RPF_2, and RPF_3 containing obvious influential components are selected. Finally, the original signal is judged by the method of envelope demodulation. In Figure 8, it is found that the frequency corresponding to the maximum peak value of 0.07 is 155.30 Hz by using envelop analysis.

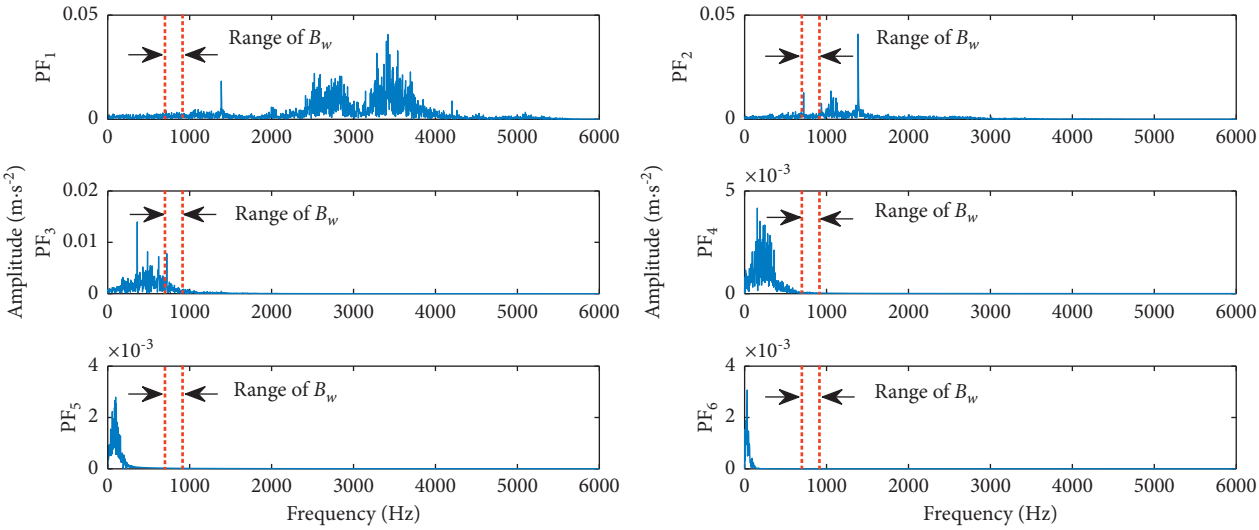

Figure 5: Calculated PF components with the ELMD algorithm for the benchmark dataset.

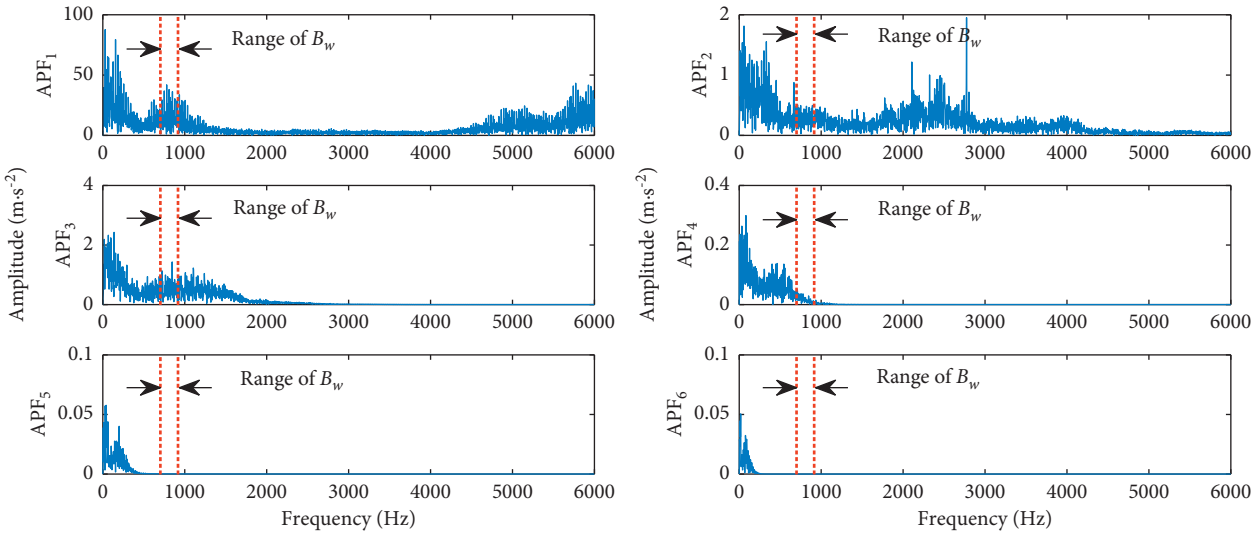

Figure 6: Calculated PF components with the reinforced ELMD algorithm for the benchmark dataset.

According to the way given in [26] by using the physical mechanism with known parameters listed in Table 1, the real fault frequency of the deep groove ball bearing of SKF 6205-2RS is estimated as follows:

$$f = \frac{r}{60}\frac{1}{2}E\left(1 + \frac{d}{D}\cos\alpha\right), \tag{7}$$

where r is the bearing speed, E stands for the number of rolling elements, d is the rolling element diameter, D is the bearing pitch diameter, and α presents the contact angle.

According to the values given in Table 1, the real fault frequency is calculated as 156.00 Hz. Consequently, the estimation error between the proposed method and the real value is 0.70 Hz. For comparison, the traditional "manual selection," "LMD + FSK," and "ELMD + FSK" strategies are employed. For manual selection, only component PF_1 is selected, and the other five PF components will be missed, which will affect the accuracy of the final diagnosis result. For the ELMD + FSK strategy, component PF_3 plotted in Figure 5 is selected because a large amplitude is observed in the frequency band frequency range [693.33 Hz, 906.67 Hz]. Although other components also contain fault frequency, their vibration amplitudes are too small to be considered. Similar results could be observed for "LMD + FSK-based approach."

To comprehensively evaluate the proposed method, more fault scenarios are compared in Table 2, including inner fault under other rotating speeds and the outer fault with different rotating speeds. Computing the error ratio through dividing the error from its real value, it is observed that the proposed method could give the accurate fault frequency with a large amplitude. Specifically, for the outer fault with high rotating speed, errors of the proposed method are much smaller in comparison with the other methods.

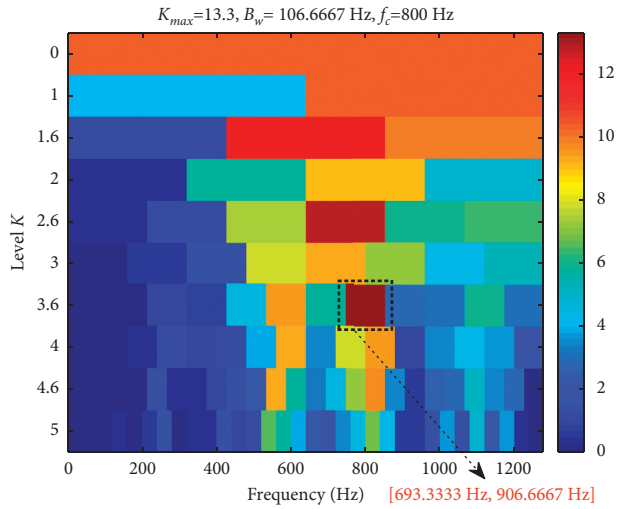

Figure 7: FSK map of the inner fault of the SKF 6205-2RS deep groove ball bearing.

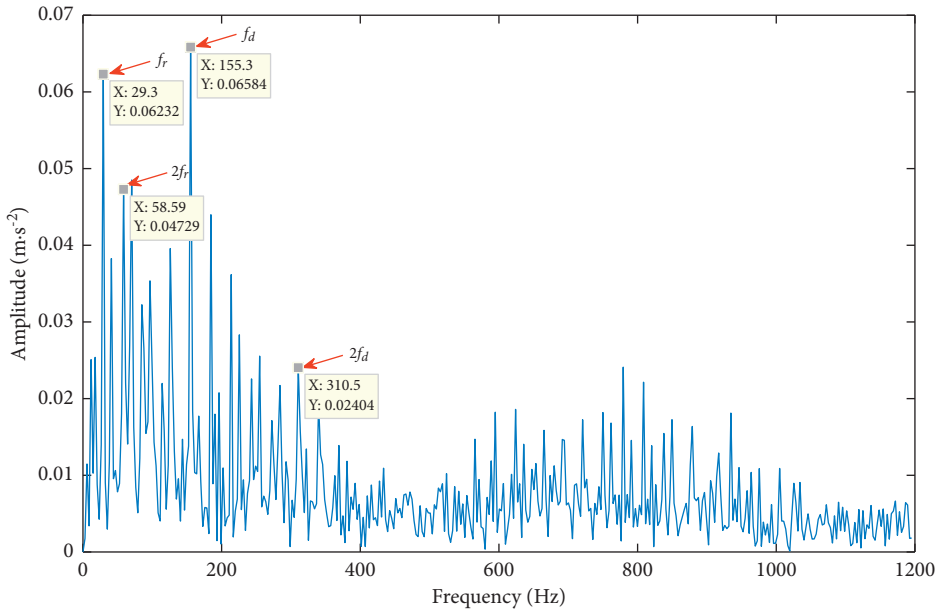

Figure 8: Envelop analysis of the reconstructed signal only using the selected components.

Table 2: Identification accuracy comparisons between the proposed method and its counterparts under different operating conditions of CWRU dataset.

Fault	Speed	Fault frequency	Rule of thumb			LMD + FSK			ELMD + FSK			Reinforced ELMD + FSK (proposed)		
			CFF (Hz)	Error (%)	AFF	CFF (Hz)	Error (%)	AFF	CFF (Hz)	Error (%)	AFF	CFF (Hz)	Error (%)	AFF
Inner	1730	156.03	155.30	0.46	0.22	155.27	0.49	0.07	155.30	0.46	0.21	155.30	**0.46**	**6.49**
	1750	157.84	158.20	0.23	0.18	158.20	0.23	0.08	158.20	0.23	0.17	158.20	**0.22**	**12.78**
	1772	159.82	158.20	1.02	0.15	161.13	0.82	0.07	158.20	1.01	0.15	158.20	**1.01**	**17.87**
	1797	162.08	161.10	0.60	0.18	161.13	0.59	0.09	161.10	0.60	0.18	161.10	**0.60**	**40.30**
Outer	1730	103.47	108.40	4.76	0.01	102.53	0.91	0.01	108.40	4.76	0.01	108.40	**4.76**	**4.87**
	1750	104.66	93.75	10.42	0.02	93.75	10.42	0.01	105.50	0.80	0.01	105.50	**0.80**	**6.45**
	1772	105.98	158.20	49.27	0.01	70.31	33.66	0.01	158.20	49.27	0.01	99.68	**5.94**	**2.49**
	1797	107.47	131.80	22.64	0.01	131.84	22.68	0.02	128.90	19.94	0.01	102.50	**4.62**	**5.41**

CFF indicates the calculated fault frequency of a certain method. AFF denotes the amplitude at fault frequency of the corresponding method.

Table 3: Performance comparisons under strong background noise by decreasing SNR to 1/5 of the original data from CWRU dataset.

Fault	Speed	Fault frequency	Rule of thumb			LMD + FSK			ELMD + FSK			Reinforced ELMD + FSK (proposed)		
			CFF (Hz)	Error (%)	AFF	CFF (Hz)	Error (%)	AFF	CFF (Hz)	Error (%)	AFF	CFF (Hz)	Error (%)	AFF
Inner	1730	156.03	181.60	16.39	0.10	210.94	35.19	0.24	181.60	16.39	0.12	158.17	**1.37**	**102.80**
	1750	157.84	249.00	57.75	0.11	219.73	39.21	0.23	249.00	36.61	0.13	160.43	**1.64**	**31.72**
	1772	159.82	360.40	125.50	0.10	219.94	31.99	0.24	166.69	4.29	0.11	166.69	**4.29**	**112.20**
	1797	162.08	219.70	26.23	0.10	199.22	22.91	0.22	194.88	20.24	0.09	161.10	**0.61**	**117.40**
Outer	1730	103.47	260.70	135.55	0.03	260.70	160.31	0.03	284.20	174.67	0.04	99.61	**3.73**	**19.50**
	1750	104.66	149.40	42.75	0.07	187.50	79.15	0.21	105.50	0.80	0.03	105.50	**0.80**	**8.50**
	1772	105.98	184.60	74.18	0.03	199.22	87.98	0.20	184.60	74.18	0.03	108.40	**2.28**	**8.10**
	1797	107.47	351.60	227.16	0.04	134.76	25.39	0.22	87.89	18.22	0.04	102.50	**4.62**	**13.81**

CFF denotes the calculated fault frequency. AFF denotes the amplitude at fault frequency.

Table 4: Performance comparisons under strong background noise by decreasing SNR to 1/6 of the original data from CWRU dataset.

Fault	Speed	Fault frequency	Rule of thumb			LMD + FSK			ELMD + FSK			Reinforced ELMD + FSK (proposed)		
			CFF (Hz)	Error (%)	AFF	CFF (Hz)	Error (%)	AFF	CFF (Hz)	Error (%)	AFF	CFF (Hz)	Error (%)	AFF
Inner	1730	156.03	503.90	222.95	0.11	123.05	33.31	0.11	209.56	33.31	0.11	162.22	**3.97**	**182.10**
	1750	157.84	395.50	150.57	0.11	134.77	14.62	0.22	163.59	3.64	0.12	163.59	**3.64**	**23.67**
	1772	159.82	199.20	24.64	0.10	169.92	6.32	0.20	169.30	5.93	0.10	169.30	**5.93**	**88.53**
	1797	162.08	334.00	106.07	0.13	190.80	17.83	0.14	190.80	17.83	0.14	181.90	**12.20**	**482.10**
Outer	1730	103.47	187.50	81.21	0.03	114.26	10.43	0.22	131.80	27.38	0.04	99.61	**3.73**	**81.63**
	1750	104.66	474.60	353.47	0.03	111.30	6.34	0.04	111.30	6.34	0.04	108.40	**3.57**	**49.44**
	1772	105.98	202.10	90.69	0.03	111.33	5.05	0.23	99.68	5.94	0.04	108.40	**2.28**	**43.31**
	1797	107.47	345.70	221.67	0.04	99.61	7.31	0.28	128.90	19.94	0.03	108.40	**0.87**	**37.70**

CFF denotes the calculated fault frequency. AFF denotes the amplitude at fault frequency.

To evaluate the performances of each method under noisy environment, two different scenarios are compared by adding Gaussian white noise in different degrees. Here, SNR is reduced to 1/5 and 1/6 of the original signal, respectively. Although the original signal has been largely weakened, the proposed method still could accurately identify fault frequency in most cases. Especially for the outer fault with a rotating speed of 1750 r/min, the performance of the proposed method remained the same and was not influenced by noise. The detailed results are given in Tables 3 and 4.

3.2. Experimental Results with a Practical Platform. Based on the SIEMENS-LMS Test Lab multichannel data acquisition instrument and the diagnostic comprehensive test platform of Spectra Quest, we developed a testing system as shown in Figure 9 to collect vibration data of the rolling bearing. The experimental data were further used to verify the efficacy of the proposed algorithm.

First of all, the American ER-12K rolling bearing with outer ring failure was installed near the input end of the coupling [27, 28], as shown in Figure 10. The basic parameters of the rolling bearing are listed in Table 5. In the experiment, a PCB608A11 accelerometer was used to collect the vibration signals in the vertical direction of the bearing seat with a sampling frequency of 25600 Hz and a motor speed of 3100 r/min. One group of time-domain signals is shown in Figure 11.

Next, ELMD is performed on the time-domain waveform of the ER-12K rolling bearing to obtain six PF components, and then their frequency spectrum is calculated as shown in Figure 12. The proposed enhancement algorithm is used to enhance the six PF components mentioned above, and the corresponding spectrum is illustrated in Figure 13.

Figure 14 shows the FSK diagram of the time-domain waveform of the ER-12K rolling bearing. It is observed that the center frequency f_c and the bandwidth B_w corresponding to the maximum kurtosis $K_{\max}$ are 4800 Hz and 3200 Hz, respectively. According to the frequency band ranging from 3200 Hz to 6400 Hz in the black dashed box, two components APF_1 and APF_2 containing prominent impact components are selected.

The real fault frequency is calculated by the envelope demodulation method, which is 122.08 Hz for the outer ring fault frequency with the parameter listed in Table 6. In Figure 15, it is found that the frequency corresponding to the maximum peak value of 0.002 is 118.75 Hz. Therefore, the estimation error of the proposed method is 3.33 Hz, which is about 2.73%.

The manual selection strategy and the ELMD + FSK strategy are further adopted for comparison. Only the component PF_1 will be selected for manual selection, inevitability leading to the poor fault diagnosis of the following analysis. For the ELMD + FSK strategy, components PF_1 and PF_2 plotted in Figure 12 are selected as crucial ones because large amplitude is observed in the frequency range from

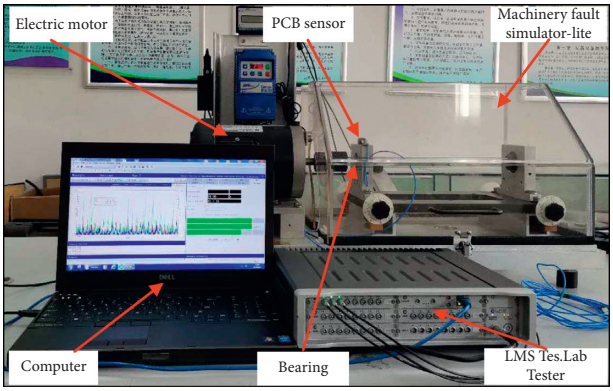

Figure 9: Flow diagram of the proposed fault diagnosis methodology.

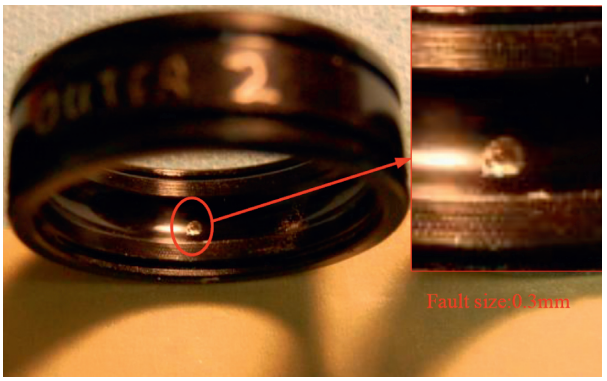

Figure 10: The tested bearings with failure on the outer ring fault.

Table 5: Specifications of American ER-12K cylindrical roller bearing with outer ring fault.

Parameter name	Values	Unit
Bearing inner diameter	19.00	mm
Bearing outer diameter	47.00	mm
Number of rolling elements (E)	8.00	1
Rolling element diameter (d)	7.90	mm
Pitch circle diameter (D)	33.50	mm
Contact angle (α)	0.00	degree

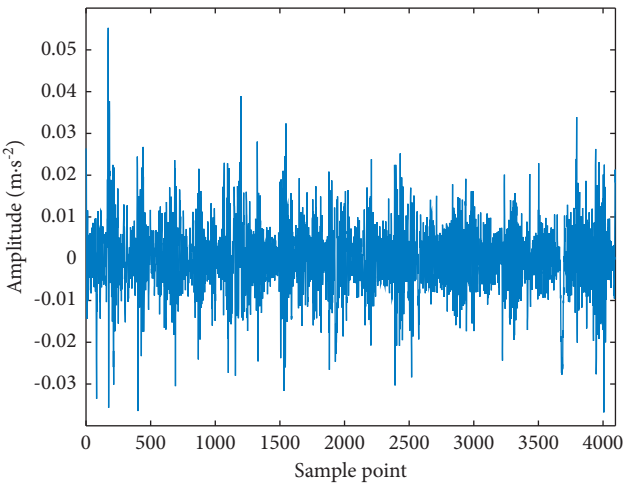

Figure 11: The time-domain trend of the employed data collected from ER-12K deep groove ball bearing with outer ring fault.

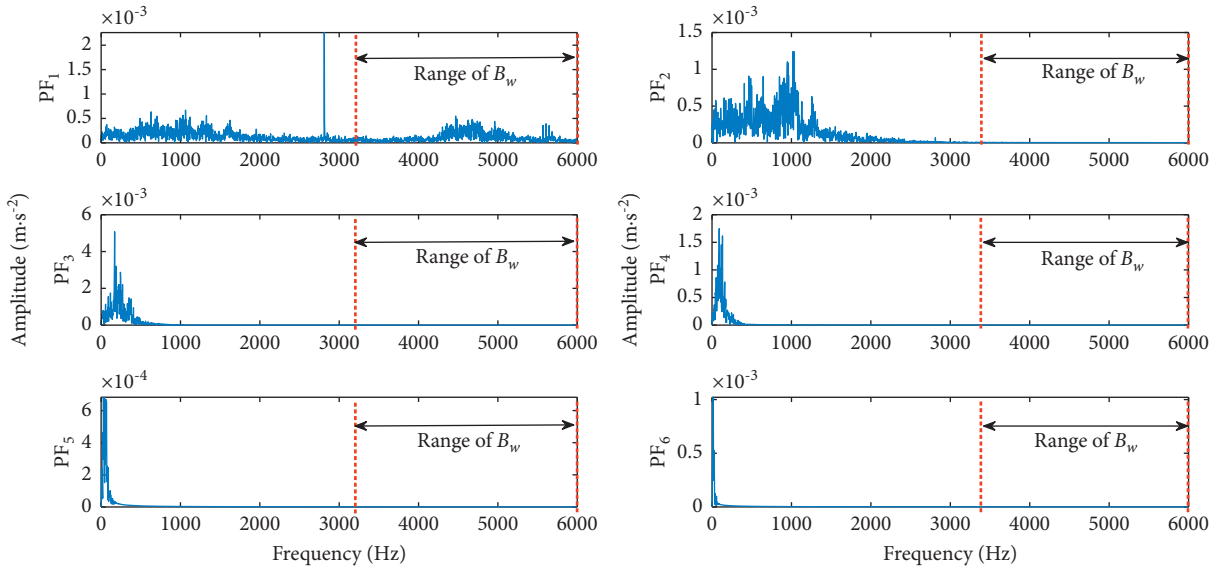

Figure 12: Calculated PF components with the ELMD algorithm for the experimental dataset.

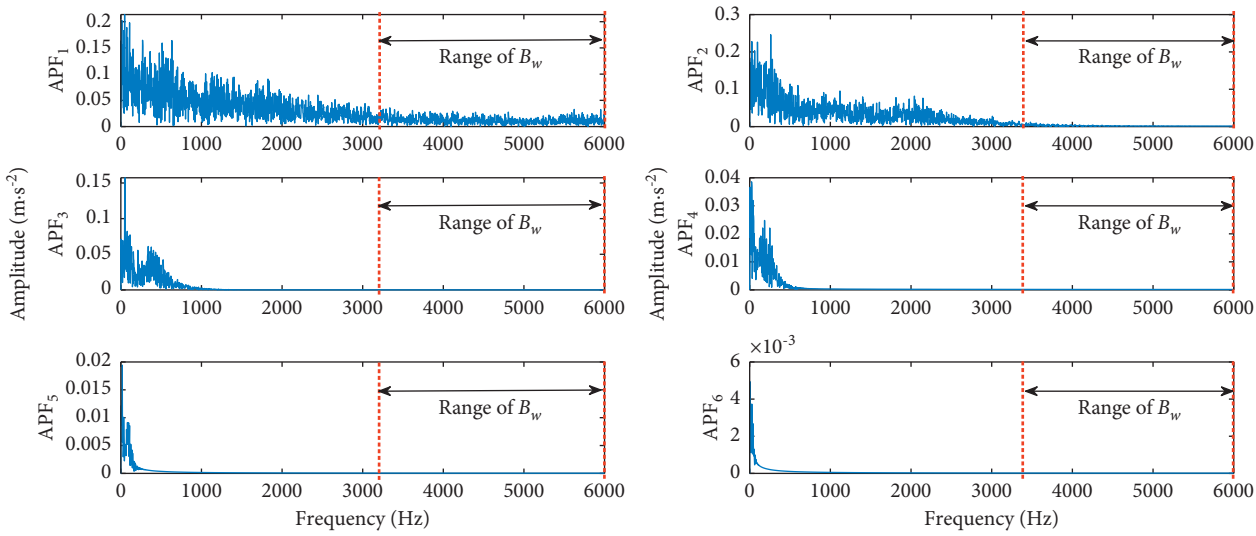

Figure 13: Calculated PF components with the reinforced ELMD algorithm for the experimental dataset.

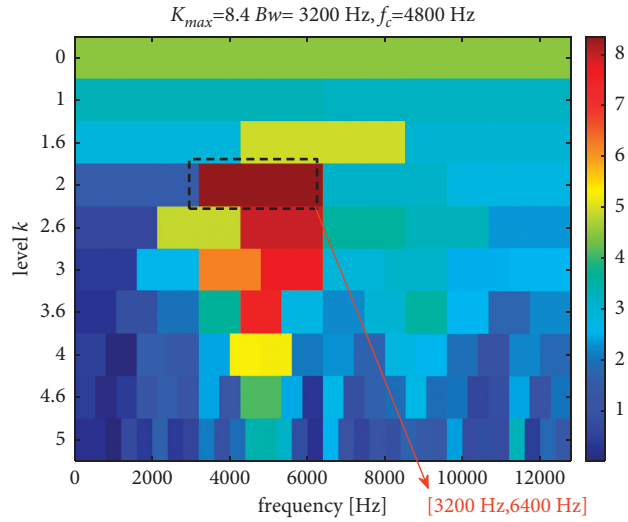

Figure 14: FSK map of the ER-12K bearing with outer ring fault.

Table 6: Performance comparisons for the proposed method using experimental data from ER-12K rolling bearing.

Real fault frequency	Rule of thumb			LMD + FSK			ELMD + FSK			Reinforced ELMD + FSK (proposed)		
	CFF (Hz)	Error (%)	AFF	CFF (Hz)	Error (%)	AFF	CFF (Hz)	Error (%)	AFF	CFF (Hz)	Error (%)	AFF
122.08 Hz	112.50	7.85	0.003	112.50	7.85	0.004	131.25	7.52	0.001	118.75	2.73	0.002

CFF denotes the calculated fault frequency. AFF denotes the amplitude at fault frequency.

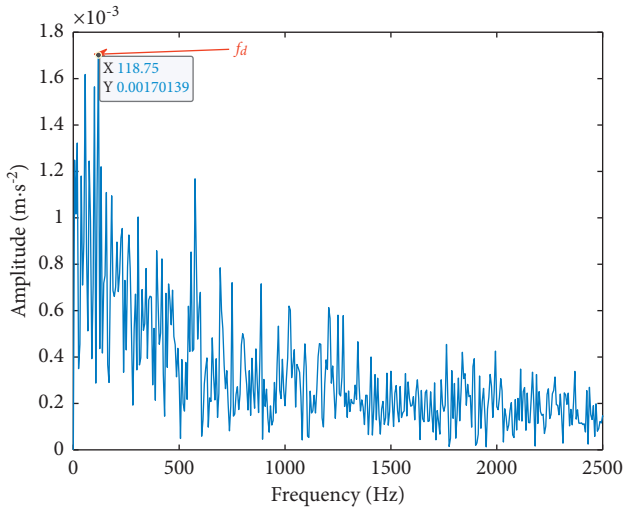

Figure 15: Envelop analysis of the reconstructed signal only using the selected components.

3200 Hz to 6000 Hz. Although other components also contain fault frequency, their vibration amplitudes are very weak. As a result, some crucial components will be missed for the manual selection and the ELMD + FSK strategy. Similar results could be observed for "LMD + FSK-based approach."

4. Conclusion

Accurate identification of fault frequency for rolling bearing remarkably influences the overall performance of machinery processes. This study presents a reinforced ensemble local mean decomposition method to address the drawbacks of the traditional ensemble local mean decomposition method in handling the fault signals. Especially, strong ambient noise easily masked faulty signs of rolling bearings, resulting in inaccurate identification or even totally missing the real fault frequencies. We use ELMD to decompose the vibration signal into a series of preliminary features, and then the frequency components above the average level are energy-enhanced through the proposed mechanism. After that, the decomposed faulty components could be identified with the fast spectral kurtosis algorithm. The experimental results indicate that the proposed model outperforms other baseline models.

Data Availability

The time-series data used to support the findings of this study are currently under embargo while the research findings are commercialized. Requests for data, six months after publication of this article, will be considered by the corresponding author.

Conflicts of Interest

The authors declare that they have no conflicts of interest.

Acknowledgments

This research was supported by the National Natural Science Foundation of China (nos. 51865045 and 61903327), Natural Science Foundation of Inner Mongolia (no. 2017MS0509), and Inner Mongolia Scientific Research Projects of Colleges and Universities (no. NJZY19298).

References

[1] Y. Du, Y. Chen, G. Meng, J. Ding, and Y. Xiao, "Fault severity monitoring of rolling bearings based on texture feature extraction of sparse time-frequency images," *Applied Sciences*, vol. 8, no. 9, p. 1538, 2018.

[2] A. AlShalalfeh and L. Shalalfeh, "Bearing fault diagnosis approach under data quality issues," *Applied Sciences*, vol. 11, p. 3289, 2021.

[3] Z. Feng, D. Zhang, and M. J. Zuo, "Adaptive mode decomposition methods and their applications in signal analysis for machinery fault diagnosis: a review with examples," *IEEE Access*, vol. 5, pp. 24301–24331, 2017.

[4] X. Ding, Q. Li, L. Lin, Q. He, and Y. Shao, "Fast time-frequency manifold learning and its reconstruction for transient feature extraction in rotating machinery fault diagnosis," *Measurement*, vol. 141, pp. 380–395, 2019.

[5] X. Zhang, Q. Han, Z. Peng, and F. Chu, "A comprehensive dynamic model to investigate the stability problems of the rotor-bearing system due to multiple excitations," *Mechanical Systems and Signal Processing*, vol. 70-71, pp. 1171–1192, 2016.

[6] N. E. Huang, Z. Shen, S. R. Long et al., "The empirical mode decomposition and the Hilbert spectrum for nonlinear and non-stationary time series analysis," *Proceedings of the Royal Society A: Mathematical, Physical & Engineering Sciences*, vol. 454, no. 1971, pp. 903–995, 1998.

[7] H. Li, T. Liu, X. Wu, and Q. Chen, "Application of EEMD and improved frequency band entropy in bearing fault feature extraction," *ISA Transactions*, vol. 88, pp. 170–185, 2019.

[8] S. S. Jonathan, "The local mean decomposition and its application to EEG perception data," *Journal of The Royal Society Interface*, vol. 2, no. 5, pp. 443–454, 2005.

[9] B. Pang, G. Tang, T. Tian, and C. Zhou, "Rolling bearing fault diagnosis based on an improved HTT transform," *Sensors*, vol. 18, no. 4, p. 1203, 2018.

[10] Q. Xiong, Y. Xu, Y. Peng, W. Zhang, Y. Li, and L. Tang, "Low-speed rolling bearing fault diagnosis based on EMD denoising and parameter estimate with alpha stable distribution,"

Journal of Mechanical Science and Technology, vol. 31, no. 4, pp. 1587–1601, 2017.

[11] J. Singh, A. K. Darpe, and S. P. Singh, "Bearing damage assessment using Jensen-Rényi Divergence based on EEMD," *Mechanical Systems and Signal Processing*, vol. 87, pp. 307–339, 2017.

[12] Y. Imaouchen, M. Kedadouche, R. Alkama, and M. Thomas, "A Frequency-weighted energy operator and complementary ensemble empirical mode decomposition for bearing fault detection," *Mechanical Systems and Signal Processing*, vol. 82, pp. 103–116, 2017.

[13] Y. Li, M. Xu, Y. Wei, and W. Huang, "A new rolling bearing fault diagnosis method based on multiscale permutation entropy and improved support vector machine based binary tree," *Measurement*, vol. 77, pp. 80–94, 2016.

[14] S. Wang, P. Niu, Y. Guo et al., "Early diagnosis of bearing faults using decomposition and reconstruction stochastic resonance system," *Measurement*, vol. 158, Article ID 107709, 2020.

[15] L. Wang, Z. Liu, Q. Miao, and X. Zhang, "Time-frequency analysis based on ensemble local mean decomposition and fast kurtogram for rotating machinery fault diagnosis," *Mechanical Systems and Signal Processing*, vol. 103, pp. 60–75, 2018.

[16] X. Zhang and J. Zhou, "Multi-fault diagnosis for rolling element bearings based on ensemble empirical mode decomposition and optimized support vector machines," *Mechanical Systems and Signal Processing*, vol. 41, no. 1-2, pp. 127–140, 2013.

[17] Z. J. He and Z. X. Zhou, "Fault diagnosis of roller bearings based on ELMD sample entropy and Boosting-SVM," *Vibration and shock*, vol. 35, no. 18, pp. 190–195, 2016.

[18] C. Wang, H. Li, J. Ou, and G. Huang, "Early weak fault diagnosis of gearbox based on ELMD and singular value decomposition," in *Proceedings of the 2019 Prognostics and System Health Management Conference*, pp. 1–5, Qingdao, China, 2019.

[19] N. Tandon and A. Choudhury, "A review of vibration and acoustic measurement methods for the detection of defects in rolling element bearings," *Tribology International*, vol. 32, no. 8, pp. 469–480, 1999.

[20] Y. B. Tang, *Research on the Mechanical Characteristics of High-Speed Rolling Bearings for Aero-Engines*, Nanjing University of Aeronautics and Astronautics, Nanjing, China, 2005.

[21] P. K. Kankar, S. C. Sharma, and S. P. Harsha, "Rolling element bearing fault diagnosis using wavelet transform," *Neurocomputing*, vol. 74, no. 10, pp. 1638–1645, 2011.

[22] J. Antoni and R. B. Randall, "The spectral kurtosis: application to the vibratory surveillance and diagnostics of rotating machines," *Mechanical Systems and Signal Processing*, vol. 20, no. 2, pp. 308–331, 2006.

[23] W. A. Smith and R. B. Randall, "Rolling element bearing diagnostics using the Case Western Reserve University data: a benchmark study," *Mechanical Systems and Signal Processing*, vol. 64-65, pp. 100–131, 2015.

[24] X. Li, W. Zhang, Q. Ding, and J.-Q. Sun, "Multi-Layer domain adaptation method for rolling bearing fault diagnosis," *Signal Processing*, vol. 157, pp. 180–197, 2019.

[25] L. Zhang, L. Guo, H. L. Gao, D. W. Dong, G. Q. Fu, and X. Hong, "Instance-based ensemble deep transfer learning network: a new intelligent degradation recognition method and its application on ball screw," *Mechanical Systems and Signal Processing*, vol. 140, pp. 1–14, 2020.

[26] J. H. Yang, *Practical Technology of Rolling Bearing Diagnosis Field*, Mechanical Industry Press, Beijing, China, 2015.

[27] Y. Liu, Z. Jiang, H. Huang, and J. Xiang, "Asymmetric penalty sparse model based cepstrum analysis for bearing fault detection," *Applied Acoustics*, vol. 165, Article ID 107288, 2020.

[28] Y. Liu, Z. Jiang, H. Huang, and J. Xiang, "A TEO-based modified Laplacian of Gaussian filter to detect faults in rolling element bearing for variable rotational speed machine," *IET Science, Measurement & Technology*, vol. 15, no. 2, pp. 193–203, 2021.